

# Lab #2: Pulsed NMR

Kevin O'Brien

April 8, 2019

## Abstract

The experiment performed in this lab followed the pulsed NMR method to determine spin-spin relaxation and spin-lattice relaxation constants of mineral oil, CuSO<sub>4</sub>, and a sample of our own creation. For the spin-lattice relaxation and spin-spin relaxation constants of mineral oil we found values of T<sub>1</sub>= 50.9± 3.27 ms, and T<sub>2</sub> = 5.417± 0.278 ms. For CuSO<sub>4</sub> we found a variety of these time constants for increasing molarity, and we found that as the molarity increases, values of these constants inverted appear to increase with an almost linear trend, with all values tabulated below. For our own sample we have found values of T<sub>1</sub>= 775±255 ms and T<sub>2</sub>= 5.599±1.59 ms.

# 1 Introduction

Nuclear magnetic resonance, or NMR as it is abbreviated, was first observed by Edward Purcell and Felix Bloch and is used to "study the conformational, structural, and dynamic properties of a wide variety of molecular and biological systems" according to ACS.com [4]. At the time, Purcell and Bloch utilized what is now called continuous wave nuclear magnetic resonance, however in the 1950s, Erwin Hahn introduced Pulsed NMR. In the original case that Purcell and Bloch studied, continuous wave NMR was performed by tuning a radio-frequency oscillator to "beat" against the resonance of a nuclear magnetic moment in a magnetic field, however in the case that we are studying in this lab, pulsed NMR, we are using a series of radio frequency pulses at  $180^\circ$  and  $90^\circ$  pulses to observe what are called "free induction decays" and "spin echoes" [3]. Since its inception, pulsed NMR has found great commercial success, and it is now the primary technology used in MRI, or magnetic resonance imaging. In this experiment, we aim to study the mechanisms behind pulsed NMR through studying the effect of magnetic pulses through samples of mineral oil,  $\text{CuSO}_4$ , and our own created sample. Through these measurements, we will hope to arrive at values of the characteristic time constants  $T_1$  and  $T_2$  of the materials which are the spin-lattice relaxation times and the spin-spin relaxation times respectively. These values will help us understand the way the protons in these materials reach resonance, which can allow us to learn a lot about the composition of the materials.

# 2 Theory

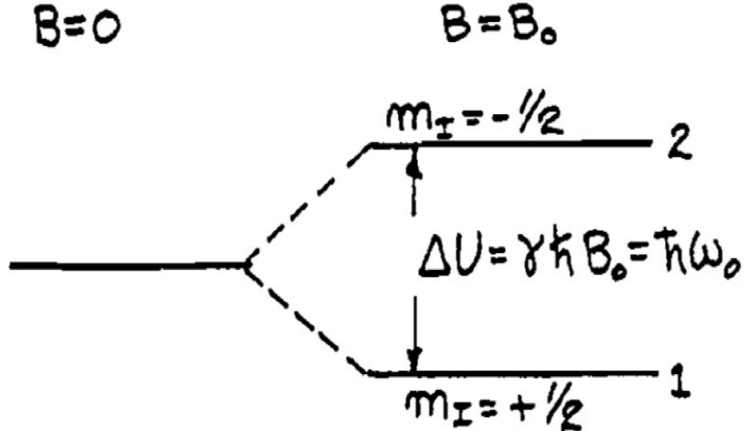
Pulsed NMR begins with the visualization of the nucleus of the hydrogen atom as a spinning bar magnet. This bar magnet has a magnetic moment  $\vec{\mu}$  and angular momentum  $\vec{J}$  such that  $\vec{\mu} = \gamma \vec{J}$  where  $\gamma$  is a quantity known as the gyromagnetic ratio. The angular momentum can be defined as  $\vec{J} = \hbar \vec{I}$  with  $\hbar$  being Planck's constant, which is the proportionality constant that quantizes the angular momentum, and  $\vec{I}$  being the spin of the nucleus. Since the nucleus is magnetic, it has a magnetic energy that is equal to the negative of the strength of the magnetic field multiplied by the magnetic moment. For the z direction of the magnetic field, we find that the energy  $U$  is equal to  $U = -\vec{\mu}_z \cdot \vec{B}_0 = -\gamma \hbar I_z B_0$ , where  $I_z$  can equal the spins of the proton in the nucleus, which are  $\pm 1/2$ . We thus find the difference in the two allowed energy states of the proton in the magnetic field to be represented by the below image. We also find a linear relationship between the constant magnetic field applied, and the proton resonance frequency using this difference in energy states to be  $f_0 = 4.258 B_0$ .

Within a particular sample containing  $N_1$  spins per unit volume in the first state, and  $N_2$  spins per unit volume in the second state, we find an expression for thermal equilibrium given by the Boltzmann factor which is

$$\frac{N_2}{N_1} = e^{-\Delta U/kT} = e^{-\hbar\omega_0/kT}$$

and the magnetization would be  $M_Z = (N_1 - N_2)\mu$ . For  $N$  magnetic moments (the sum of the number of moments in each state), we find that the thermal

Figure 1: Energy separation between the two magnetic energy states [Taken from 1]



equilibrium magnetization per unit volume is  $M_0 = N\mu \tanh(\frac{\mu B}{kT}) \approx N \frac{\mu^2 B}{kT}$ . We find that it takes a certain number of time for the magnetization to build up to equilibrium in the system, and in the case of the z-component of the magnetic field, this build up time is exponential. We find the equation relating the magnetic field strength in the z direction to this spin-lattice relaxation time  $T_1$  to be

$$M_z(t) = M_0(1 - e^{-t/T_1})$$

Before a particular sample is placed in the magnetic field, the number of protons in the  $N_1$  and  $N_2$  states are equal, and upon reaching thermal equilibrium it is found that more are in the lower energy state than the higher energy state.

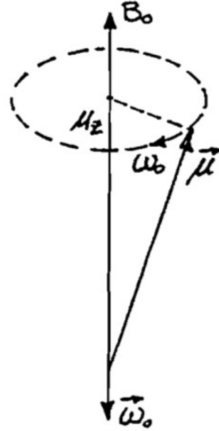
We find that in thermal equilibrium there is only net magnetization in the  $M_z$  direction, which can be explained through the idea of the torque,  $\vec{\tau}$  on the loop. In this case,  $\vec{\tau} = \frac{d\vec{J}}{dt}$  where the torque also equals  $\vec{\mu} \times \vec{B}$ . Thus we have  $\vec{\mu} \vec{B} = \frac{1}{\gamma} \frac{d\vec{\mu}}{dt}$ . We see that the system precesses as shown in the figure below.

Since the only magnetization that we can measure a signal of through the oscilloscope is in the transverse plane, we must find a way to produce temporary magnetic fields in the x and y planes through the use of radio frequency pulsed magnetic fields. We find that such a rotating magnetic field can be written of the form

$$B_{eff}^* = B_1 \hat{i}^* + (B_0 - \frac{\omega}{\gamma}) \hat{k}^*$$

In a rotating magnetic field of frequency  $\omega_0$  we find that  $\frac{\omega}{\gamma} = B_0$  or  $\omega = \gamma B_0 = \omega_0$ . This yields a constant magnetic field in the  $x^*$  direction and the magnetization precesses about the magnetic field. Certain pulses at specific angles will change the direction of the magnetic field, for example if the magnetization reaches a peak in the transverse plane, that is a  $90^\circ$  pulse, where  $M_z \rightarrow M_y$ . A  $180^\circ$  pulse arises when the magnetization is rotated back into the z direction, and results in a magnetization that is  $-M_z$ . A full  $360^\circ$  pulse brings the magnetization back to its original  $M_z$  on the z-axis. When a  $90^\circ$  pulse is applied on a sample, we find that there is a net magnetization in the x-y plane, however

Figure 2: Precession of the magnetic moment in a magnetic field [Taken from 1]



this net magnetization only persists for a quantity of time that is defined by an exponential equation. The spin-spin relaxation time  $T_2$  defines the relaxation time of the system's transverse magnetization. The equations to model the magnetization as it relates to this spin-spin relaxation time are given via the equations

$$M_{x*}(t) = M_0 e^{-t/T_2}$$

and

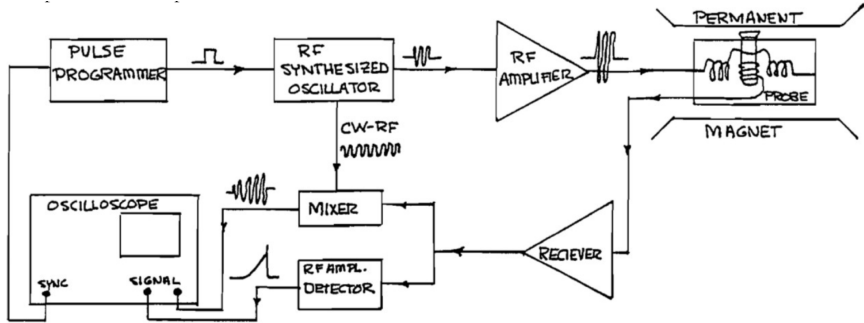
$$M_{y*}(t) = M_0 e^{-t/T_2}$$

By plotting the decay of  $M_x$  after a  $90^\circ$  pulse, we can arrive at the value of  $T_2$ , using a signal known as the free induction decay. For the case of the PS1-A magnet which we use, at its magnetic sweet spot, the  $T_2$  is equal to the free induction decay. The experiment we will go on to perform will allow us to measure these spin echoes and free induction decays to calculate these values.

### 3 Experimental Set-Up

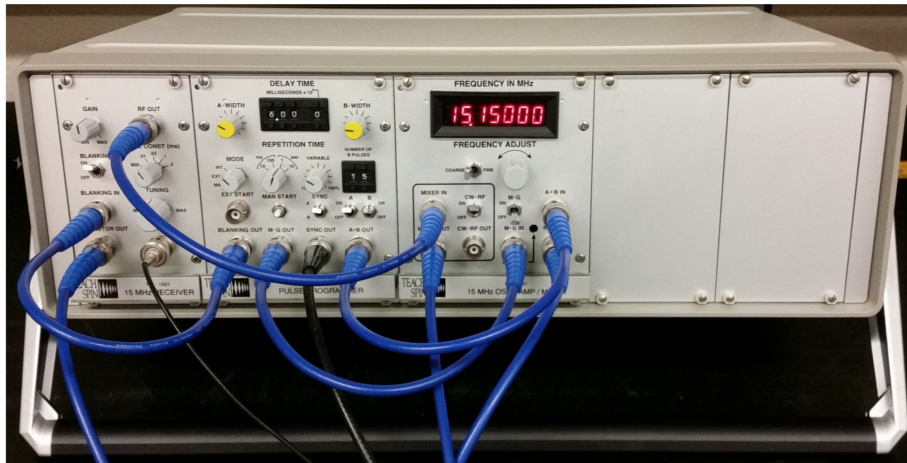
The set up for this experiment requires primarily the use of TeachSpin's PS1-A pulsed NMR spectrometer. The block diagram for the set up is featured below

Figure 3: Block diagram of the experimental set-up [Taken from 1]



The block diagram shows a pulse programmer, an RF synthesized oscillator, mixer, an RF amplifier, a receiver, a permanent magnet and the oscilloscope which is used to take the measurements of data for this experiment. This diagram functions by the pulse programmer creating a pulse stream that gates the synthesized oscillator into radio frequency pulse bursts and triggers the oscilloscope. The RF current in the coil produces a homogeneous 12 gauss rotating magnetic field. This produces the precession of the magnetization in the form of the 90° and 180° pulses. The magnet used is incredibly strong and the digitally synthesized oscillator produces a stable frequency. The transmitter coils in the magnet carriage are wound in a Helmholtz configuration to optimize the RF magnetic field homogeneity.

Figure 4: Controller unit [Taken from 1]



The controller unit shown above holds the pulse programmer, and the RF circuitry while the magnet assembly holds the sample vials and connects to the control unit. When nuclear magnetization precesses transverse to the constant

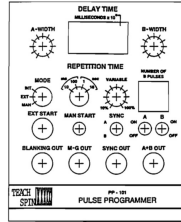
Figure 5: Magnet assembly [Taken from 1]



magnetic field, an EMF is induced in the receiver coil which is amplified by the receiver circuitry. Upon being amplified, it can be detected by the RF amplitude detector which rectifies the signal and outputs a signal proportional to the RF precessional signal's peak amplitude. It is also detected by a mixer which is used to multiply the precession signal with the master oscillator. Rather than its output being proportional to the peak amplitude, it is proportional to the difference between the two frequencies. The mixer is used to set the frequency of the oscillator to the proton resonant frequency. This frequency can be observed as a zero beat output on the oscilloscope. The magnet has a clear plastic cover, which should remain closed for the most part as changes in temperature can affect the proton resonant frequency of the system. Additionally, magnetic parts should be kept away from the magnet as they can degrade the homogeneity of the magnet.

Within the control unit is a pulse programming module. This module creates the pulses that will be used for the experiment, within which we can vary the mode of observation, the delay time, the signal width, and the number of B pulses. The front panel of the pulse programmer is shown below

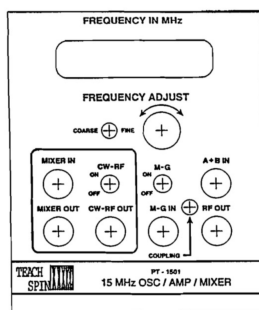
Figure 6: Pulse programmer [Taken from 1]



The next module contains the oscillator, amplifier and mixer. The first part,

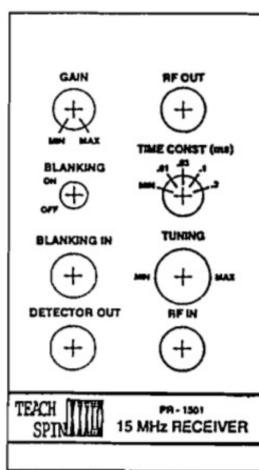
the oscillator contains a crystal oscillator that is accurate to one part in a million over a half hour. The frequency of the oscillator can be controlled with the fine and coarse dials, and this value is displayed on the screen. The next part of this module is the amplifier, which amplifies the pulse bursts to produce the constant 12 gauss magnetic field that is incident on the sample. The final part of this module, the mixer, multiplies the continuous wave RF signal from the oscillator with the RF signals from the precessing nuclear magnetization. The mixer is the reason for the beat signal shown on the oscillator, which when properly adjusted should show no beats. The front panel of this module is shown below

Figure 7: Oscillator, amplifier and mixer [Taken from 1]



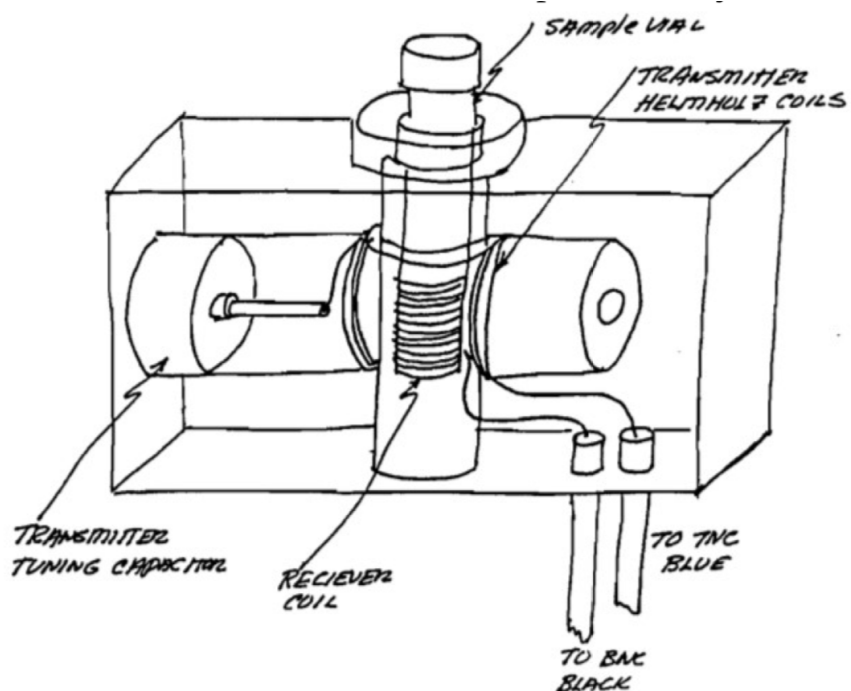
The last module is the 15 MHz receiver. This module recovers rapidly from overloads and amplifies the radio frequency induced EMF from the magnetization. This receiver connects to the coils wrapped around the sample vials within the sample probe. The module then amplifies and detects the tiny induced voltage. This signal goes directly into the oscilloscope. The front panel can be seen below. It features a tuning knob which rotates the variable air capacitor, and a gain knob.

Figure 8: 15 MHz receiver [Taken from 1]



The final required part of the set up is the sample probe shown below which consists of a transmitter coil and a receiver pick up coil. The transmitter coil is in a Helmholtz configuration with its axis perpendicular to the perpendicular to the magnetic field, while the receiver coil is wound up in a solenoid configuration. An EMF is induced in this coil which is amplified by the receiver and observed by the oscilloscope.

Figure 9: Sample probe [Taken from 1]



## 4 Procedure

The first six parts of the experiment will be mostly qualitative in nature as we will be observing the uses and functions of the controller unit, as we familiarize ourselves with the various methods of generating pulses.

### 4.1 Pulse Programmer

To begin the experiment, we will familiarize ourselves with the pulse programmer. For this A pulse, we will use the settings given in the lab manual, ensuring that the circuits have all been properly connected. From here, we will use the oscilloscope trigger menu, and set it up for an external sync pulse trigger that is positively sloped. The sweep time setting can be set to 5.00, 10.0 or 25.0  $\mu\text{s}/\text{div}$  and 1.00 V/div for the amplitude setting. From here, various parameters are changed to observe their changes to the pulse. The A-width knob is varied to see how that affects the pulse, as well as setting the repetition time to 10 ms, and the oscilloscope sweep time to 2.50 ms/div. We then observe the changes to the pulse brought on by changing the variable for repetition time from 10% to 100%. Lastly, we switch the mode from Int to Man, and press the Man-start button to see what occurs.

### 4.2 Pulse Sequences

For the next part of the experiment, we are moving to a two pulse sequence. For this, we must turn the B-switch to the on position, and set the number of B pulses on the control unit to 1, as well as setting the delay time to 100  $\mu\text{s}$ . For this portion of the experiment, the A and B width settings can be set to arbitrary values, as they will be adjusted. The sweep time on the oscilloscope should be set to 50.0  $\mu\text{s}/\text{div}$ , and again 1.00 V/div for the amplitude. We then observe changes as the A and B widths, the delay time, repetition time and sync are changed, as well as turning off the A and or B signals. The oscilloscope sweep time is then changed to 1.00 ms/div and the pulses are observed as delay time is increased.

### 4.3 Multiple Pulse Sequences

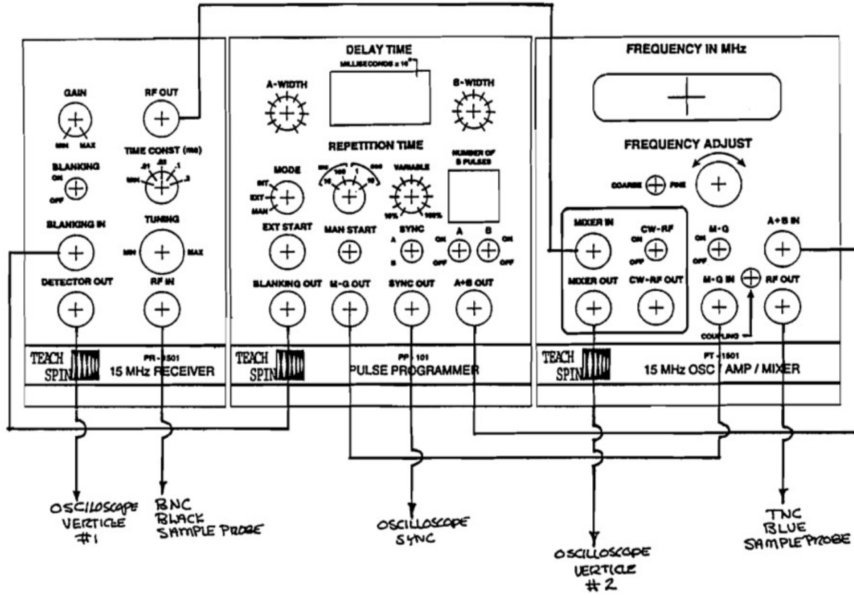
Next, we will observe an A pulse, with multiple B pulses rather than just one. This case will utilize three pulses. To accomplish this, we set the number of B pulses to 2, and use the remaining settings from the lab manual to achieve the desired pulse signal. The oscilloscope is set to a sweep time 250  $\mu\text{s}/\text{div}$  and the amplitude is still held at 1.00 V/div. Once these have been set, the number of B pulses is varied from 3 to 10. Next the mode is switched to Man, and the Man-start button is pressed. We change the delay time to 2.00 ms, and set the sweep time to 1.00 ms/div and observe the changes in precision of the image.

### 4.4 The Spectrometer

Use the figure below to connect the spectrometer modules to each other, and the spectrometer to the oscilloscope using BNC cables. The TNC connector in the RF out is used to connect the power amplifier to the transmitter coils in

the sample probe. This TNC connector is to remain connected at all times to avoid damaging the system.

Figure 10: Connections of the control unit [Taken from 1]



#### 4.5 The Receiver

A crucial step in this lab is setting the receiver in the control unit to its resonant frequency. In order to set the receiver to this frequency, a sample is required. We place the prepared sample of mineral oil in the magnet assembly. The oscilloscope is set to a sweep time of  $500 \mu\text{s}/\text{div}$  and  $1.00\text{V}/\text{div}$  amplitude. The gain knob on the receiver is set to about 50% and the tuning knob is varied in order to produce a maximum signal on the oscilloscope. A ballpark estimate of the resonant frequency is provided on the label on the magnet, however this is subject to change based on temperature or other factors, thus we must find the resonant frequency experimentally. Using the mixer out signal, we set the frequency of the pulse programmer such that it reaches the proton resonance frequency of the magnet. This device resets the frequency whenever it is turned off, so this resonance frequency must be reset every time the machine is turned back on. Additionally, the resonant frequency is subject to change with time as the temperature is increased. Thus it should be periodically checked throughout the experiment to ensure accuracy of data.

#### 4.6 Free Induction Decay

For this part of the experiment we will be observing the free induction decay signal which is due to the magnetization precessing about the applied constant magnetic field in the x-y plane. In order to observe the free induction decay, we must create transverse magnetization by applying a high power RF pulsed

magnetic field to the sample over a period of time that causes the thermal equilibrium magnetization to precess  $90^\circ$  in the rotating frame. After this, the precession signal decays to zero in a time that is determined by the spin-spin relaxation time  $T_2$ . For the mineral oil sample, we must set the repetition time to 500 ms. In order to set a  $90^\circ$  pulse, we must set the value of the A width such that it arrives at the shortest width that produces maximum signal. This happens when the A width is at around 20%. The remaining settings for the control unit can be taken from the lab manual. After this has been achieved, an oscilloscope screenshot can be taken.

#### 4.7 Magnetic Field Contours

After we have observed the Free Induction Decay, or FID, we will now examine the contours of the electric field. To do this, we will use the controls on the side of the sample carriage which moves the sample in the x-y plane. Upon changing the vials position in the carriage, a new resonance frequency is to be measured by beating the frequency against the master oscillator's frequency. This frequency can then be recorded, and using equation 7, we can calculate the magnetic field strength at each location. These measurements should be taken relatively quickly in order to avoid temperature changing within the carriage. We will then construct a plot of magnetic field as a function of position in the x-y plane.

#### 4.8 Rotating Coordinate Systems

For this part of the experiment, we will examine whether or not a signal can be observed when the frequency of the spectrometer is not tuned to resonance. First, we tune the spectrometer to resonance, and then vary the frequency of the oscillator to about 0.7 MHz upfield and downfield of the resonant frequency. Then the frequency is to be changed until no signal appears. The pulse widths can then be varied to try to observe pulses off resonance. We then draw diagrams of the effective fields in the rotating frame off resonance.

#### 4.9 Spin Lattice Relaxation Time, $T_1$

Now, we must find a way to determine the time constant that characterizes the exponential growth of the magnetization towards thermal equilibrium in a static magnetic field,  $T_1$ . We can first estimate  $T_1$  by reducing the FID to 1/3 of its maximum value. This is done by lowering the repetition time, which does not allow the magnetization to return to its thermal equilibrium value before the next  $90^\circ$  pulse. The signal being reduced to about 1/e gives a good estimate for the value of  $T_1$ . A more accurate way to measure  $T_1$  comes from programming a pulse sequence of  $180^\circ - \tau$  (variable) -  $90^\circ$ . By varying the delay time  $\tau$ , we can observe the growth of the magnetization towards its equilibrium value. The second pulse is used to rotate the net magnetization into the x-y plane where it can be measurable. It is important to realize that those values of  $M_Z$  displayed on the oscilloscope are the absolute values of the actual values of  $M_Z$ . Those values of  $M_Z$  taken before it reaches zero are actually negative. The final way to measure  $T_1$  is to take about 15-20 values of  $\tau$  as the magnetization

increases to its thermal equilibrium value. Using equation 14, we can obtain a proper exponential fit of the data to determine the time constant  $T_1$ .

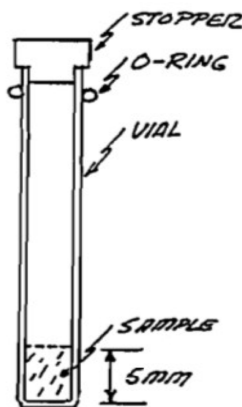
#### 4.10 Spin-spin relaxation time $T_2$

The next time constant is the spin-spin relaxation time  $T_2$ . This value represents the decay of the transverse magnetization of the system. For this experiment, we will utilize three different methods to obtain this value. The first method is a two pulse spin-echo method, similar to the one used to determine  $T_1$ . The sequence used is a  $90^\circ - \tau$  (variable) -  $180^\circ - \tau$  - echo( $2\tau$ ). As the delay time  $2\tau$  is increased, an exponential decay will be revealed. The next method for obtaining  $T_2$  is called the Carr-Purcell method. This utilizes multiple  $180^\circ$  pulses spaced a time  $\tau$  apart, and the sequence  $90^\circ - \tau - 180^\circ - 2\tau - 180^\circ - 2\tau - 180^\circ - \dots$ . We will use a small delay time, and take 15-20 measurements of echo amplitudes. This will allow us to again produce an exponential plot and determine  $T_2$ . The final method for determining  $T_2$  came as a correction to the Carr-Purcell method and it is known as the Meiboom-Gill method. This method utilizes a  $90^\circ$  phase shift between the  $90^\circ$  and  $180^\circ$  pulses which cancels the compounded error present in the Carr-Purcell sequence. Once  $T_2$  has been measured in these three ways, exponential plots should be created for each of them.

#### 4.11 CuSO<sub>4</sub> Solutions

Using the two pulse method present in 4.9 and the Meiboom-Gill method in 4.10, we will measure  $T_1$  and  $T_2$  for samples of CuSO<sub>4</sub> of molarities 1M, 0.5M, 0.2M, 0.1M, 0.05M, 0.01M and 0.005M. These are prepared using sample vials, O-rings and rubber stoppers provided on the lab table. The sample vials should be prepared such that they resemble the below image.

Figure 11: Sample vial set up [Taken from 1]



## 4.12 Natural Products

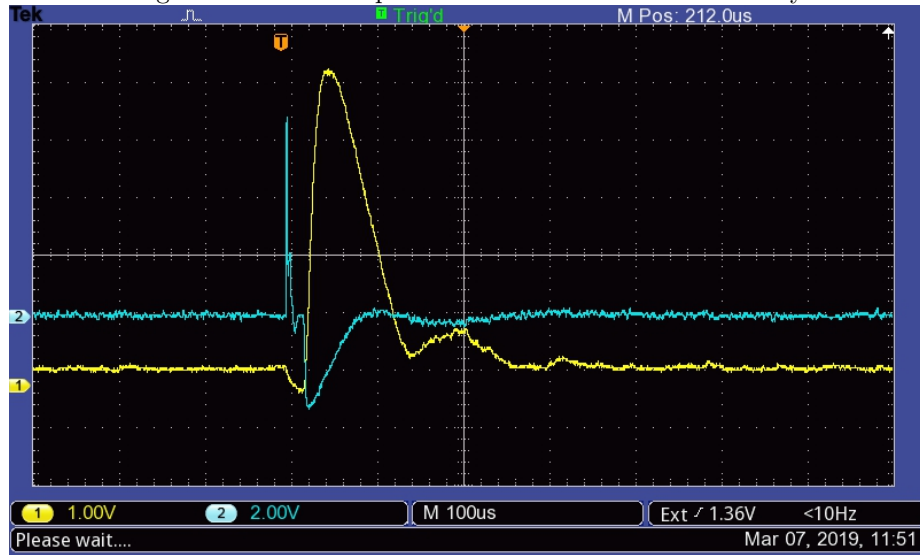
For the final part of the experiment the same process is repeated to measure  $T_1$  and  $T_2$  for a sample created. For this experiment, a sample of salt water was used.

# 5 Results

## 5.1 Free Induction Decay

The following figure is the screenshot taken from the oscilloscope of the Free Induction decay. This was obtained by using the settings from the lab manual and varying the A-width and the tuning to obtain the maximum signal of the  $90^\circ$  pulse, and then reducing the beats in the master signal so that none appear.

Figure 12: Oscilloscope screenshot of free induction decay



## 5.2 Magnetic Field Contours

In order to create a 2D field plot of the magnetic field contours, we must use equation 7 from the lab manual,

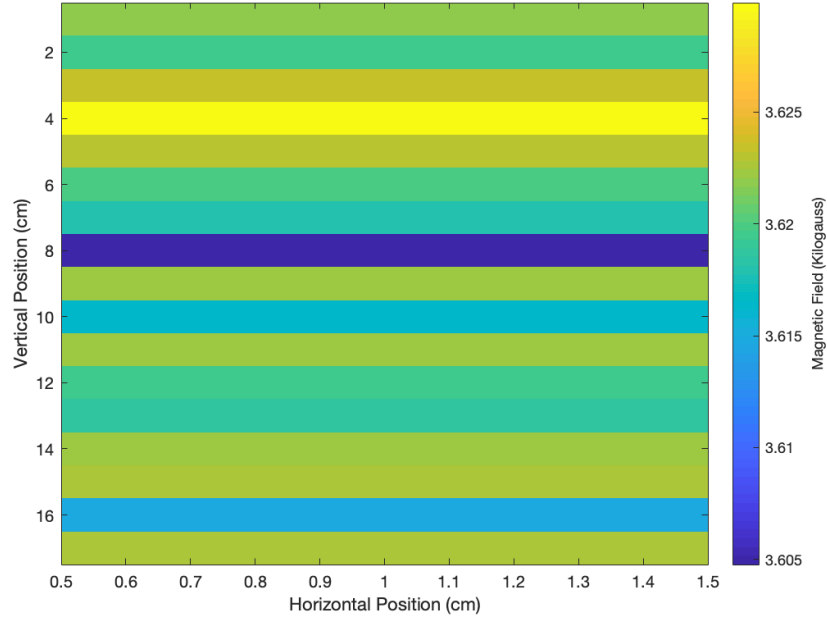
$$\omega_0 = \gamma B_0$$

This equation yields equation 9 in the manual, or

$$f_0(\text{MHz}) = 4.258B_0(\text{kilogauss})$$

We can thus take our data for frequency gathered as a function of position, and calculate values for the magnetic field at each position.

Figure 13: Magnetic field contours plot as a function of position

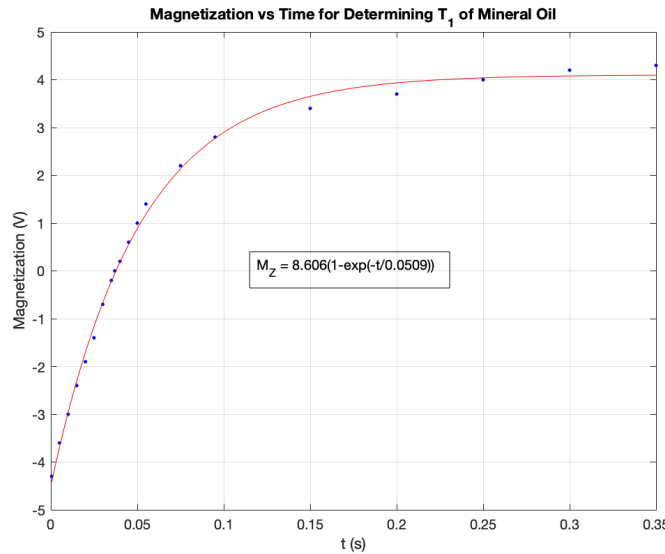


### 5.3 Calculation of $T_1$ and $T_2$ for mineral oil

For this section we are calculating the values of  $T_1$  using the two pulse sequence method, and  $T_2$  using the two pulse spin-echo method, the Carr-Purcell method, and the Meiboom-Gill method. In order to do this, we plotted the values of magnetization we measured on the oscilloscope as a function of delay time for each of the following plots, and then created an exponential fit for each plot using an appropriate function.

For  $T_1$  we have the following plot:

Figure 14: Magnetization as a function of delay time for mineral oil to measure  $T_1$



From this plot, we see that we can directly read off the value of  $T_1$  from the plot, as 50.9 ms by comparing the exponential fit function of the plot to equation 14 from the lab manual

$$M_z(\tau) = M_0(1 - e^{-\tau/T_1})$$

The exponential fit is of the form  $F(x) = a(1 - e^{x/-b})$ , and thus we arrive at our result. From the fit software we have an uncertainty of this value of  $T_1$  of 3.27 ms. Thus we can report  $T_1$  for the spin echo method of

$$T_1 = 50.9 \pm 3.27 \text{ ms}$$

In addition to this plot, we have other methods of obtaining a value of  $T_1$ , one of which is through estimation of the value by reducing the FID to about 1/3 of its total value. This estimated value was around  $90 \pm 5$  ms.

For  $T_2$ , we have the following 3 plots:

Figure 15: Magnetization as a function of delay time for mineral oil to measure  $T_2$  using spin-echo method

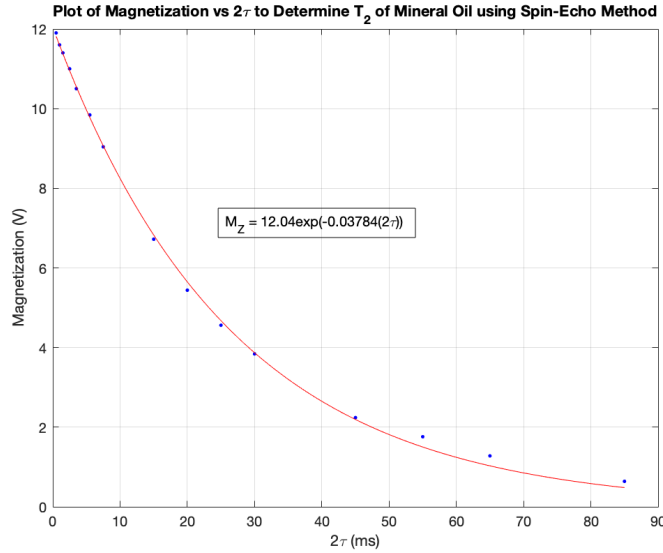
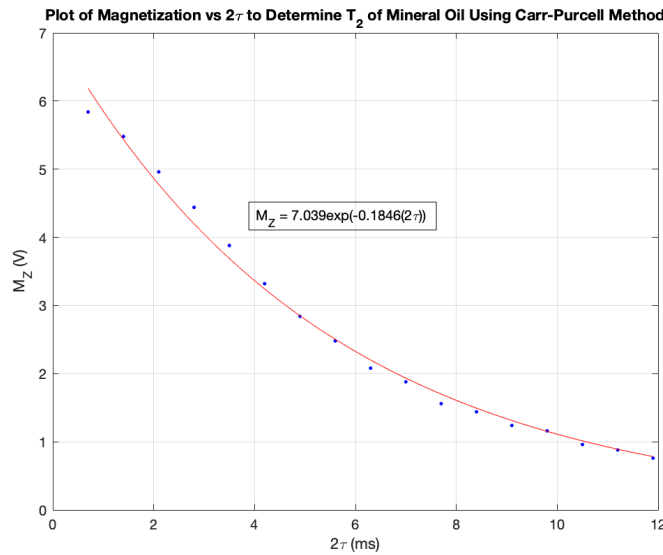
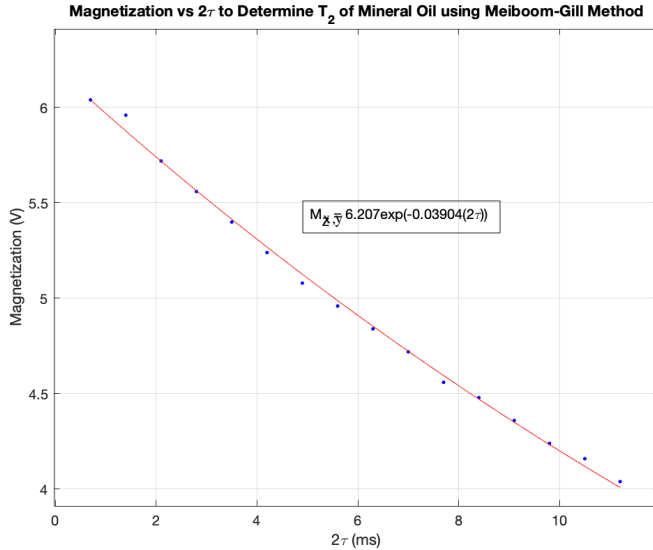


Figure 16: Magnetization as a function of delay time for mineral oil to measure  $T_2$  using Carr-Purcell method



From each of these we are able to determine a value for  $T_2$  with different degrees of accuracy. For each plot, we solve for  $T_2$  by comparing the exponential

Figure 17: Magnetization as a function of delay time for mineral oil to measure  $T_2$  using Meiboom-Gill method



fit function of each plot to equation 24 from the lab manual

$$M_{x,y}(2\tau) = M_0 e^{-2\tau/T_2}$$

From here, we see that by inverting the constant value we multiply  $2\tau$  by in our exponential fit equations we can arrive at a value for  $T_2$  for each plot. The exponential fits are of the form  $F(x) = ae^{-bx}$ , thus by taking each b value and inverting them we can arrive at values of  $T_2$ . Each b value has an uncertainty value given from the fit software which we can use to evaluate the uncertainty of the  $T_2$  values. For the spin echo method, the uncertainty in b was given as 0.00124. Evaluating the upper limit of b to solve for  $T_2$ , and then taking the difference of this value and our actual  $T_2$  value we can find the uncertainty. For the spin echo method this uncertainty is 0.841 ms. Repeating the same process for the Carr-Purcell and Meiboom-Gill methods we can report the following values.

For the first method, the spin-echo method we have  $T_2 = 26.43 \pm 0.841$  ms

For the second method, the Carr-Purcell method, we have  $T_2 = 5.417 \pm 0.278$  ms

For the third method, which in theory should be the most accurate method, we have that  $T_2 = 25.61 \pm 0.572$  ms

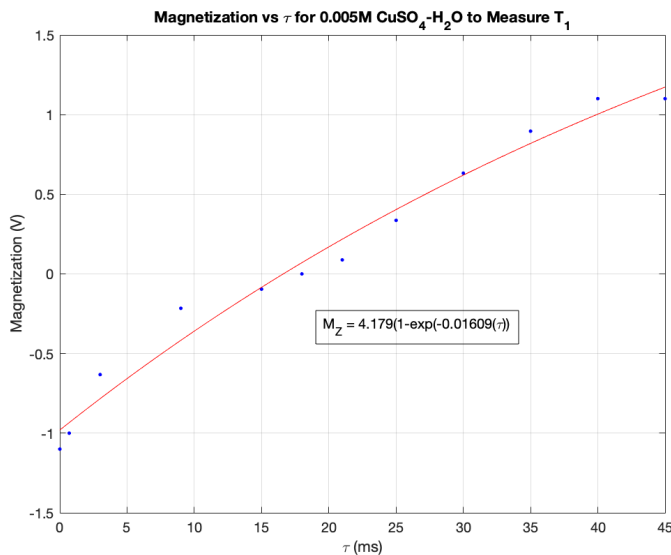
These values are consistent, as  $T_1$  should be larger than  $T_2$ , and from [2] we see that  $T_2$  should have a range of 6-60 ms and  $T_1$  should have a range between 30-150 ms. Our values from each method of measurement, aside from the Carr-Purcell method for  $T_2$ , fall within this range. This error in the Carr-Purcell method can be accounted for by the fact that the Carr-Purcell does not account for small errors in the 180° pulse generated.

## 5.4 Calculation of $T_1$ and $T_2$ for various molarities of CuSO<sub>4</sub>

### 5.4.1 $T_1$

Below are the graphs created of to measure the value of  $T_1$  for various molarities of CuSO<sub>4</sub> using the two pulse sequence method, utilizing an exponential fit of the form of the equation for the magnetization in the z-direction.

Figure 18: Magnetization as a function of delay time for 0.005 M CuSO<sub>4</sub> to measure  $T_1$



$T_1$  can be calculated from each of these plots by comparing the exponential fit function of each plot to equation 14 from the lab manual

$$M_z(\tau) = M_0(1 - e^{-\tau/T_1})$$

From here, we see that by inverting the constant value we multiply  $\tau$  by in our exponential fit equations we can arrive at a value for  $T_1$  for each plot. The exponential fits are of the form  $F(x) = a(1 - e^{-bx})$ , thus by taking our first b value from the plot of 0.005M CuSO<sub>4</sub>, which is 0.01609, and inverting it, we arrive at a value of  $T_1$  of 62.15 ms. Repeating this process for the remaining plots, we find values of  $T_1$  for increasing molarity placed in the table below in 5.4.3.

Figure 19: Magnetization as a function of delay time for 0.01 M CuSO<sub>4</sub> to measure T<sub>1</sub>

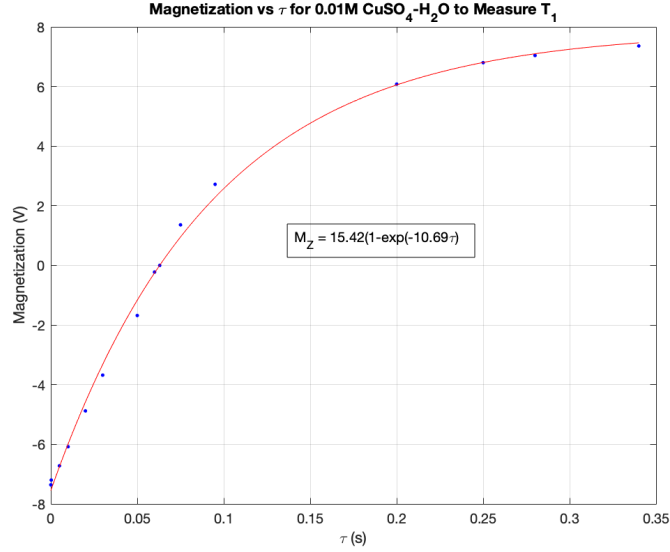


Figure 20: Magnetization as a function of delay time for 0.05 M CuSO<sub>4</sub> to measure T<sub>1</sub>

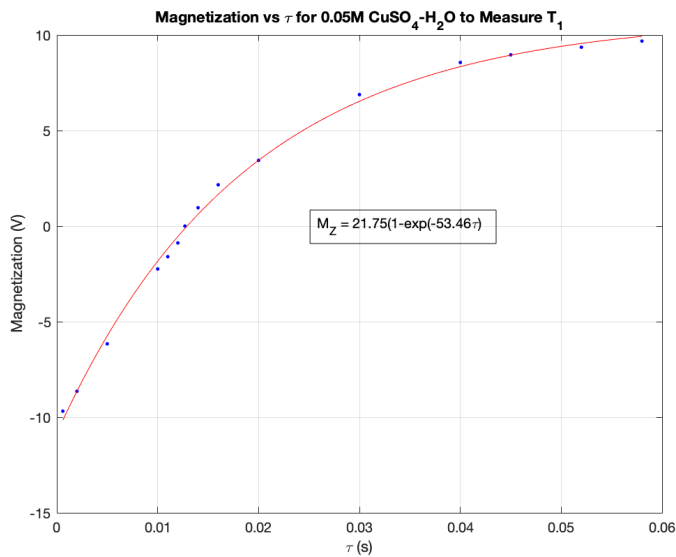


Figure 21: Magnetization as a function of delay time for 0.1 M CuSO<sub>4</sub> to measure T<sub>1</sub>

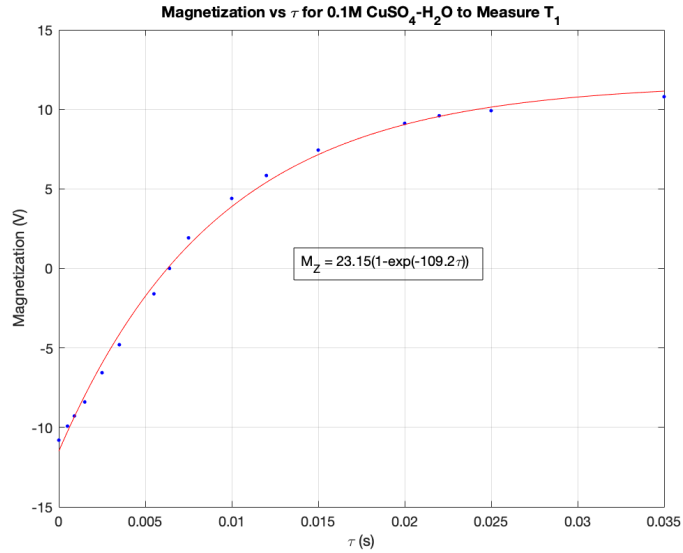


Figure 22: Magnetization as a function of delay time for 0.2 M CuSO<sub>4</sub> to measure T<sub>1</sub>

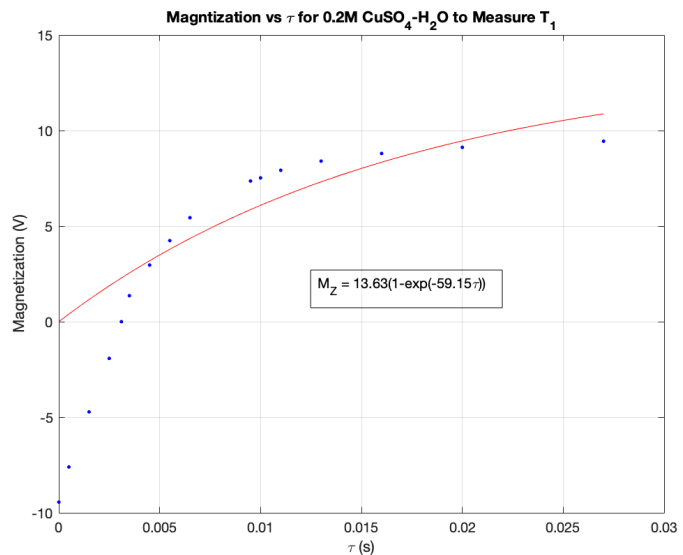


Figure 23: Magnetization as a function of delay time for 0.5 M CuSO<sub>4</sub> to measure T<sub>1</sub>

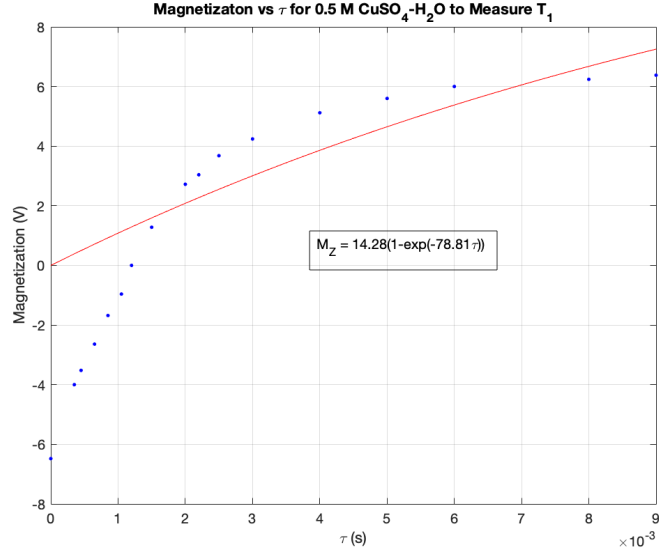
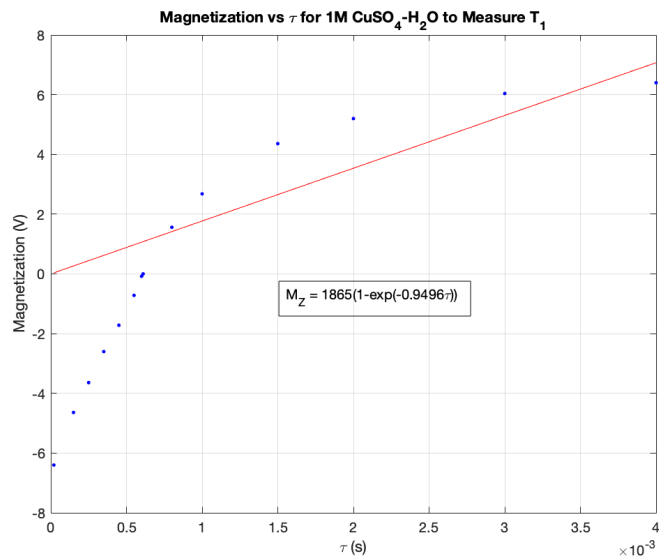


Figure 24: Magnetization as a function of delay time for 1 M CuSO<sub>4</sub> to measure T<sub>1</sub>



### 5.4.2 $T_2$

Below are the graphs created of to measure the value of  $T_2$  for various molarities of  $\text{CuSO}_4$  using the Meiboom-Gill method, utilizing an exponential fit of the form of the equation for the magnetization in the transverse plane.

Figure 25: Magnetization as a function of delay time for 0.005 M  $\text{CuSO}_4$  to measure  $T_2$

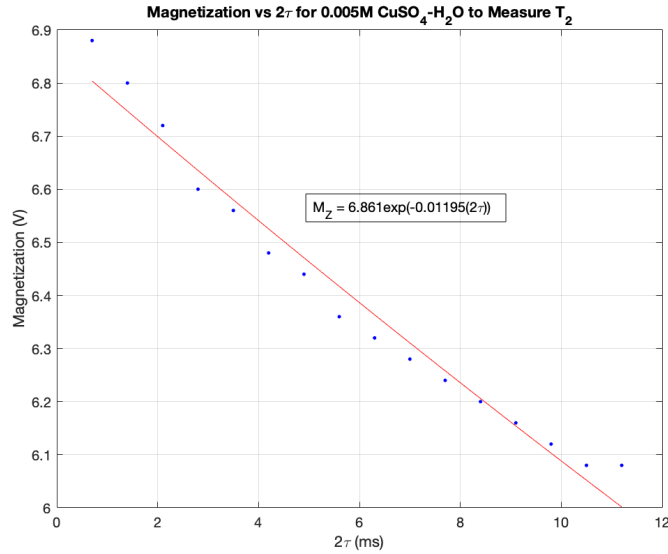


Figure 26: Magnetization as a function of delay time for 0.01 M  $\text{CuSO}_4$  to measure  $T_2$

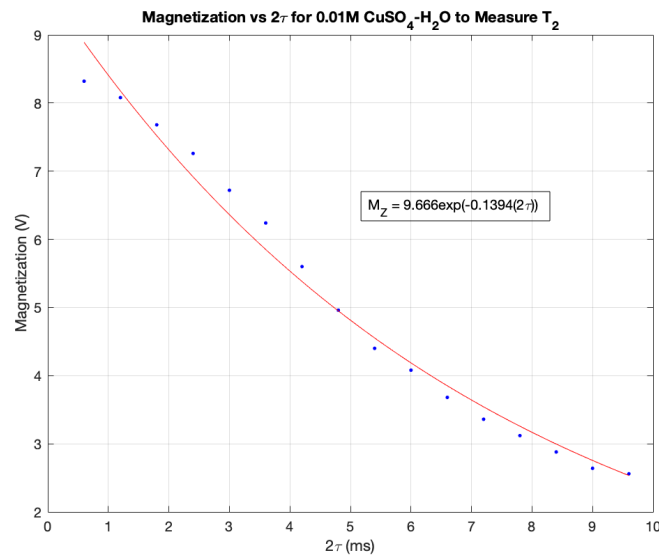


Figure 27: Magnetization as a function of delay time for 0.05 M CuSO<sub>4</sub> to measure T<sub>2</sub>

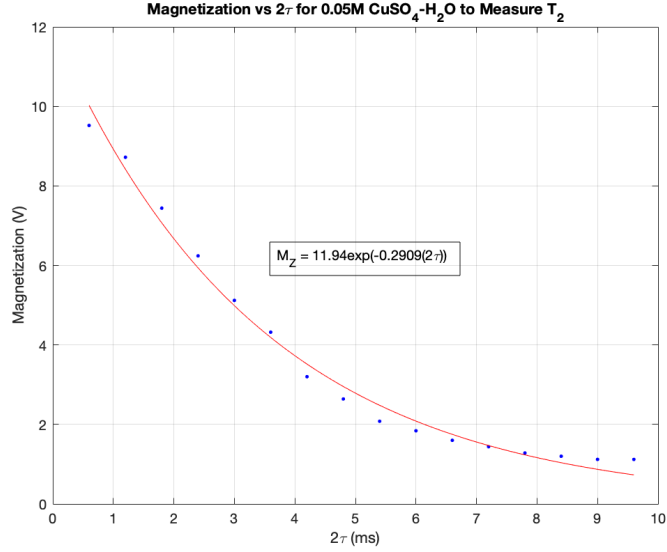


Figure 28: Magnetization as a function of delay time for 0.1 M CuSO<sub>4</sub> to measure T<sub>2</sub>

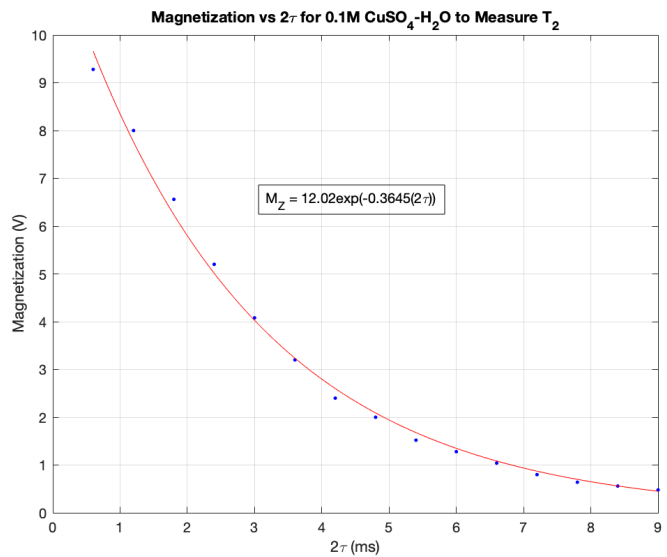


Figure 29: Magnetization as a function of delay time for 0.2 M CuSO<sub>4</sub> to measure T<sub>2</sub>

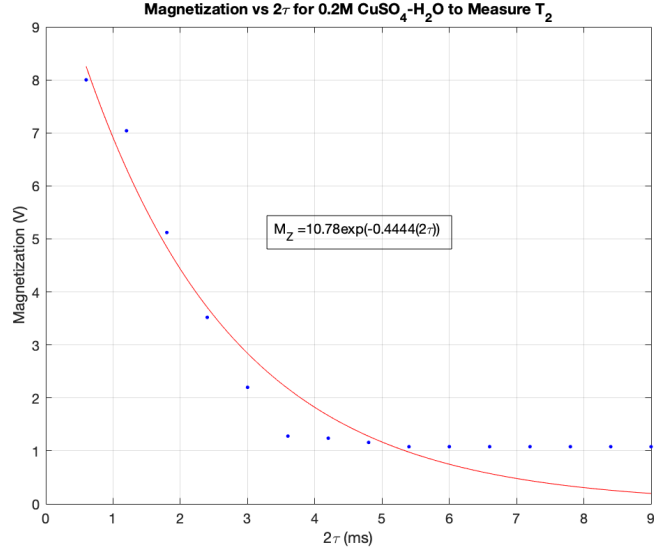


Figure 30: Magnetization as a function of delay time for 0.5 M CuSO<sub>4</sub> to measure T<sub>2</sub>

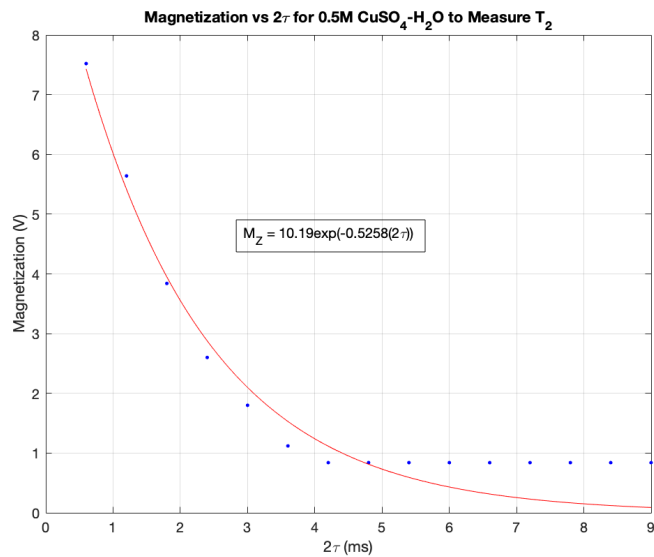
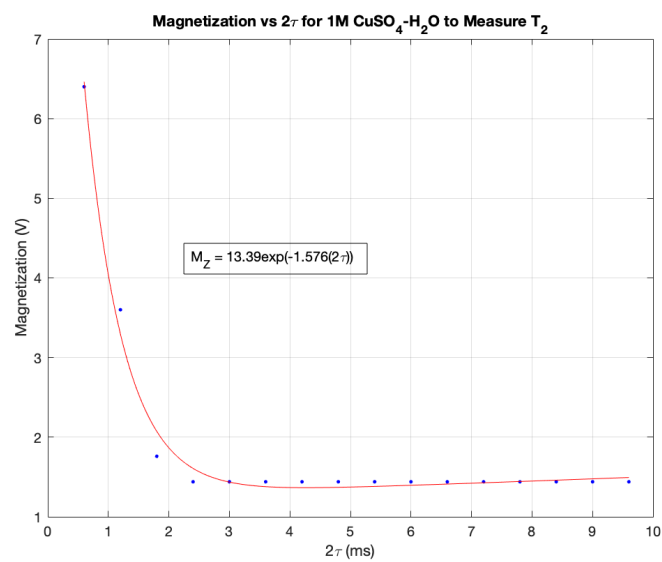


Figure 31: Magnetization as a function of delay time for 1 M CuSO<sub>4</sub> to measure T<sub>2</sub>



From these plots, we see an obvious increase in the depth of the dip taken by the exponential function as molarity increases which corresponds to a decreasing value of  $T_2$ .  $T_2$  can be calculated from each of these plots by comparing the exponential fit function of each plot to equation 24 from the lab manual

$$M_{x,y}(2\tau) = M_0 e^{-2\tau/T_2}$$

From here, we see that by inverting the constant value we multiply  $2\tau$  by in our exponential fit equations we can arrive at a value for  $T_2$  for each plot. The exponential fits are of the form  $F(x) = ae^{-bx}$ , thus by taking our first b value from the plot of 0.005M CuSO<sub>4</sub>, which is 0.01195, and inverting it, we arrive at a value of  $T_2$  of 83.68 ms. Repeating this process for the remaining plots, we find values of  $T_2$  for increasing molarity placed in the table below in 5.4.3.

### 5.4.3 Analysis of T<sub>1</sub> and T<sub>2</sub> for CuSO<sub>4</sub>

All of our values of  $T_1$  and  $T_2$  are tabulated below, with their respective uncertainties, as well as the values of  $\frac{1}{T_1}$  and  $\frac{1}{T_2}$  to create the plots of  $\frac{1}{T_1}$  and  $\frac{1}{T_2}$  as a function of molarity. Additionally, we have tabulated each of the uncertainties for values of  $T_1$  and  $T_2$  which have been calculated through the following method. For the 0.005M CuSO<sub>4</sub>, we received a constant value of 0.01195 in the  $T_2$  plot which we inverted to receive the value of  $T_2$ . The uncertainty of this value from the exponential fit was 0.00116. Thus we add this uncertainty to our value and evaluate a value of  $T_2$  at its upper limit, which comes out to 76.28 ms. From here, we subtract this from our original value of  $T_2$  to find the uncertainty. This value comes out to 6.86 ms. That value will be the uncertainty for  $T_2$  of the 0.005 M sample tabulated below.

Molarity (M)	T <sub>1</sub> (ms)	T <sub>2</sub> (ms)	1/T <sub>1</sub> (ms <sup>-1</sup> )	1/T <sub>2</sub> (ms <sup>-1</sup> )	$\sigma_{T_1}$ (ms)	$\sigma_{T_2}$ (ms)
0.005	62.15	83.68	0.01609	0.01195	29.57	6.86
0.01	93.54	7.174	0.01069	0.1394	92.5	0.521
0.05	18.71	3.438	0.05344	0.2909	1.57	0.243
0.1	9.157	2.743	0.1092	0.3646	0.8541	0.132
0.2	16.91	2.250	0.05914	0.4444	5.863	0.392
0.5	12.69	1.902	0.07880	0.5258	10.569	0.306
1	1053	0.6345	0.0009497	1.576	1052	0.0963

Table 1: Table of values to report desired quantities

From the table, we can now plot graphs of  $\frac{1}{T_1}$  vs M and  $\frac{1}{T_2}$  vs M for the two sets of data. These plots are shown below and though the plot of  $T_2$  shows a strong linearity, the plot of  $T_1$  appears very sporadic, and filled with error. However if the outlier of the 1M CuSO<sub>4</sub> is removed, it is still somewhat linear.

Figure 32:  $\frac{1}{T_1}$  vs M

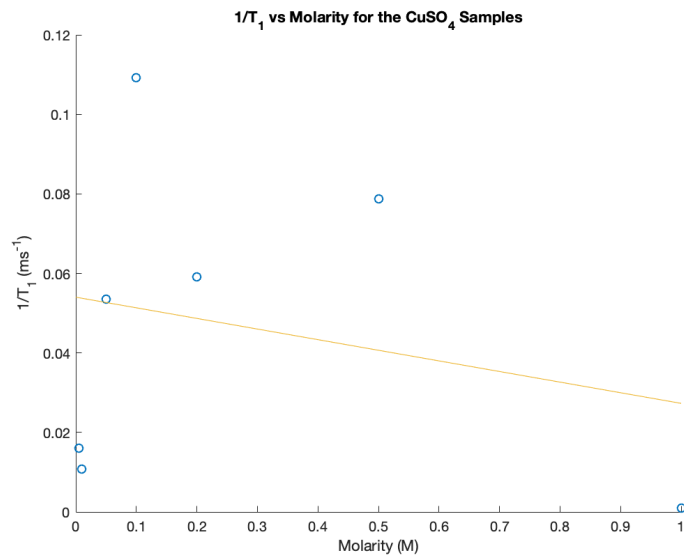
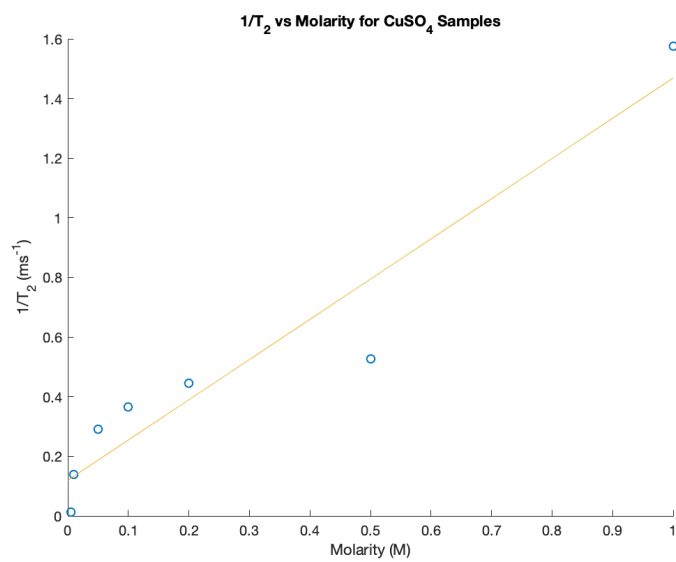


Figure 33:  $\frac{1}{T_2}$  vs M



## 5.5 Calculation of $T_1$ and $T_2$ for own sample

Figure 34: Magnetization as a function of delay time for salt water sample to determine  $T_1$

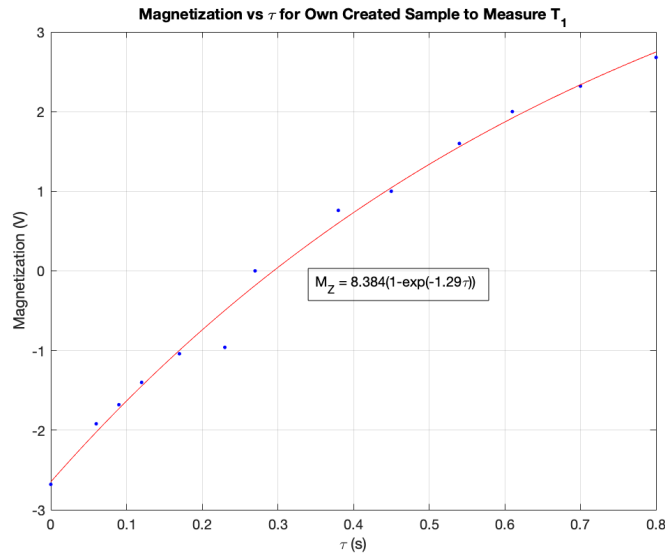
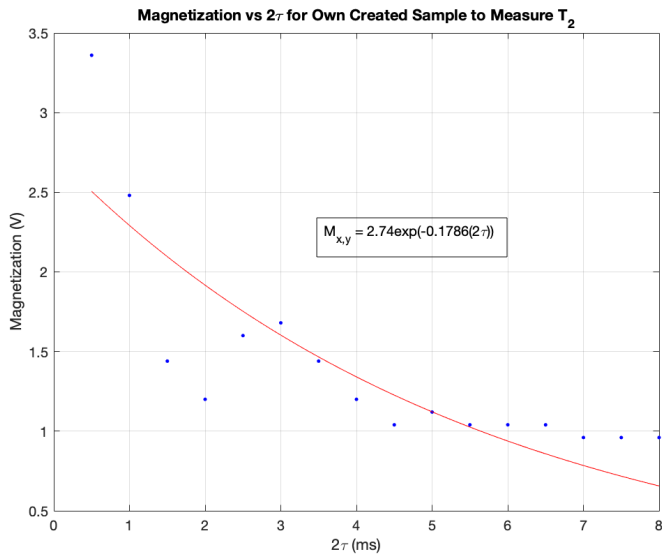


Figure 35: Magnetization as a function of delay time for salt water sample to determine  $T_2$



Using the same methods as in previous sections, we are able to use these two graphs to determine values of  $T_1$  and  $T_2$  of our own created sample. The value determined for  $T_1$  is 775 ms, and the value determined for  $T_2$  is 5.599 ms.

Once more evaluating the errors in our values in a method similar to above, we can report final values and uncertainties for our own sample to be

$$T_1 = 775 \pm 255 \text{ ms}$$

$$T_2 = 5.599 \pm 1.59 \text{ ms}$$

## 6 Summary and Conclusions

Through the data gathered in this lab we were able to utilize a variety of methods to calculate  $T_1$  and  $T_2$  for mineral oil, as well as using the two spin echo method to calculate  $T_1$  and the Meiboom-Gill method to calculate  $T_2$  for samples we prepared of  $\text{CuSO}_4$  and a sample of our own creation of salt water. In calculating  $T_1$  and  $T_2$  of mineral oil, we found values of  $T_1 = 50.9 \pm 3.27 \text{ ms}$ , and  $T_2 = 5.417 \pm 0.278$ . From [2], we find that the limits of  $T_1$  and  $T_2$  of mineral oil tend to be around 6-60 ms for  $T_2$  and 30-150 ms for  $T_1$ . Through our findings, we have found a value of  $T_1$  that is within range, and for  $T_2$  that is close to the lower limit of its range. Errors in finding experimental values for these time constants could have arisen from shifts in the proton resonance frequency that occur as temperature increases, and failure to adjust the instruments used to correct for that. Another source of error for these values could have arisen from our data points not being accurately recorded due to small changes on the oscilloscope display.

For the samples of  $\text{CuSO}_4$ , we produced many graphs of  $T_1$  and  $T_2$  at molarities which ranged from 0.005 M to 1 M. Upon fitting these plots with an appropriate exponential equation, we found that the exponential factor in the plots of  $T_2$  appeared to increase as molarity increased, leading to a larger dip in the plots. For  $T_1$  we saw a trend that was almost the opposite, as the plots appeared to become more linear as molarity was increased. Upon plotting  $1/T_1$  and  $1/T_2$ , we saw that the  $1/T_1$  plot had no apparent trend due to the presence of the outlier of the 1 M  $\text{CuSO}_4$  sample. Had this been removed, there would be a linear increase in the value of  $1/T_1$  as molarity increased. For  $1/T_2$ , our values were much more agreeable, and there was a strong linear correlation between increasing molarity and the increase in  $1/T_2$ . Perhaps to improve the values recorded for  $T_1$ , we could have used a smaller range of molarities, as the uncertainty in the exponentiality of the samples appeared to become larger and larger as molarity increased. This led to plots that were difficult for the curve fitting software to produce a proper fit of.

For the final portion of the lab, we used our own sample of salt and water to again calculate  $T_1$  and  $T_2$ , these values came out to  $T_1 = 775 \pm 255 \text{ ms}$  and  $T_2 = 5.599 \pm 1.59 \text{ ms}$ . Due to the lack of known values to compare this to, we can not compare these to any numerical data, however we can see that our exponential fit of  $T_1$  gives us a large error, which can be due to errors in measurement using the oscilloscopes measurement feature, or inhomogeneities in the magnetic field. These potential inhomogeneities also lead to strange fluctuations in our measured magnetization values for  $T_2$ .

Methods to potentially improve this experiment could be maintaining a more constant room temperature so as to prevent having to recalibrate the machinery to the proton resonant frequency, which could produce small errors in the measurements, or greater degassing of the solutions used because if they are not degassed, the presence of dissolved paramagnetic  $\text{O}_2$  gas can throw off the mea-

sured values as well [5]. A final potential error could be a failure to locate the precise magnetic "sweet spot" for the PS1-A magnet. We have found through these measurements that a majority of the time constants measured are reasonable, however due to large error, we can conclude that better exponential fits of the data can be found.

## References

- [1] Department of Physics, University at Buffalo, "Pulsed NMR."
- [2] Lee, Kent. "Pulsed NMR in Extracting Spin-Spin and Spin-Lattice Relaxation Times of Mineral Oil and Glycerol." San Diego, March 2013. [home.sandiego.edu/severn/p480w/KL\\_PNMRDraft](http://home.sandiego.edu/severn/p480w/KL_PNMRDraft)
- [3] Stoltenberg, John. "Pulsed Nuclear Magnetic Resonance." CPP, [www.cpp.edu/kvandervoort/Pulsed%20NMR%20Review.pdf](http://www.cpp.edu/kvandervoort/Pulsed%20NMR%20Review.pdf).
- [4] Lorigan, Gary A. "Teaching the Fundamentals of Pulsed NMR Spectroscopy in an Undergraduate Physical Chemistry Laboratory." Journal of Chemical Education, ACS Publications, 1 July 2001, [pubs.acs.org/doi/abs/10.1021/ed078p956](https://pubs.acs.org/doi/abs/10.1021/ed078p956).
- [5] Melville, Jonathan. "Pulse NMR Spectroscopy." Semantic Scholar, 8 Dec. 2014, [pdfs.semanticscholar.org/6fe1/a66a3880c7e26ef63f2abb3c1fd7d447eb65.pdf](https://pdfs.semanticscholar.org/6fe1/a66a3880c7e26ef63f2abb3c1fd7d447eb65.pdf).